Biophysical Journal, Volume 98

Supporting Material

Mechanism for the intracellular manipulation of organelles by conventional electroporation

Axel T. Esser, Kyle C. Smith, T. R. Gowrishankar, Zlatko Vasilkoski, and James C. Weaver

Mechanisms for the intracellular manipulation of organelles by conventional electroporation: Supplemental Information

Axel T. Esser*, Kyle C. Smith*,‡, T. R. Gowrishankar*, Zlatko Vasilkoski†, and James C. Weaver*,[1]
*Harvard-MIT Division of Health Sciences and Technology, Massachusetts Institute of Technology, Cambridge, Massachusetts

‡ Department of Electrical Engineering & Computer Science, Massachusetts Institute of Technology, Cambridge, Massachusetts

†022 Dana Research Center, Northeastern University, Boston, Massachusetts

Methods

System model for a cell with organelles. The cylindrical cell system geometry (2D cross section shown in Fig. 1 A; system depth is $d_{\mathrm{sys}} = 13.3\,\mu$m such that the present cylindrical cell volume is that of a spherical cell with 10 μm radius) includes the PM (10 μm radius), the nuclear envelope (NM; 3 μm radius) with a nuclear outer (NOM) and a nuclear inner (NIM) membrane, the membrane of the endoplasmic reticulum (ERM), and, in close proximity to the ERM (1), five mitochondria (approximated each with a $1\,\mu\mathrm{m} \times 2\,\mu\mathrm{m}$ cross sectional area), each mitochondria (MM) with a mitochondrial outer (MOM) and a mitochondrial inner (MIM) membrane, separated by 15 nm of intermembrane space. Invaginated christae of the mitochondria are taken into account by making the effective MIM area a factor $f_{\mathrm{A}} = 5$ larger than the MOM (2). NOM and NIM are separated by 10 nm, and enclose the cisterna. Further the ERM is continuous with the nucleus and has a irregular shape. Note that the organelles are in general un–evenly distributed inside the cell model. Accordingly, unlike many traditional cell models, there are no symmetries that could simplify the problem.

Modular, multiscale transport lattices (TL). The TL method maps the above cell model (or any other biological system model (2–5)) onto an equivalent electrical circuit on the basis of local models for charge transport, storage, sinks, and sources. It thus allows for the assessment of the spatial distributions of fields, potentials, membrane conductances, pores and pore size distributions on the cellular level (microdosimetry (3)). In particular, nanometer-scale membrane models M_{m} (Fig. 1 B) are constructed from modules that represent the local electrical capacitance of the membrane (C_{m}) and resting potential sources ($V_{\mathrm{ip}}, R_{\mathrm{p}}$) that give rise to membrane resting potentials of $\Delta\psi_{\mathrm{rest}}$ of -90 mV, 90 mV, and -200 mV for PM, ERM, and MIM, respectively, whereas $\Delta\psi_{\mathrm{rest}}$ for MOM, NIM, and NON are zero. (4). Passive resistances are also assigned to all membranes, lower values for the NIM, NOM, and MOM account for their leaky nature (3). Further, a dynamic current (I_{m}) takes into account the combination of the above passive current due to the static membrane resistance relevant to field exposures too small to cause EP and the dynamic pore current due to transient pores in parallel. Specifically, the EP mechanism is included in M_{m} via an

[1]Corresponding author. Fax: (617) 253-2514. Email: jcw@mit.edu.

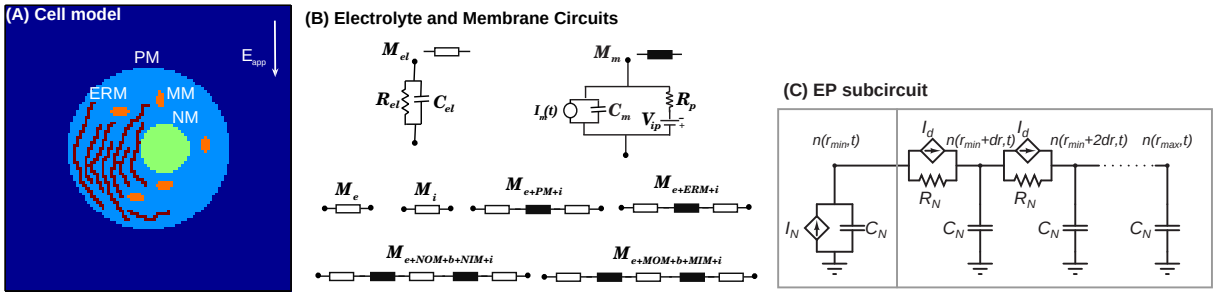

Figure 1: (A) Cross-sectional geometry of a cylindrical cell system model (radius 10 μm, depth 13.3 μm) with organelles and their associated membranes: endoplasmic reticulum (ERM), five mitochondria (MM) with outer (MOM) and inner (MIM) membranes separated by 15 nm, and a nucleus (NM) with outer (NOM) and inner (NIM) membrane separated by 10 nm; the direction of applied electric field E_{app} is indicated. (B) Local TL circuit models for electrolyte (M_{el}; open rectangle, where "el" represents extracellular (e) and intracellular (i) electrolytes, as well as the interstitial (b) electrolyte between the outer and inner membranes of the nucleus and the mitochondria) and for the membrane (M_{m}; black-filled rectangle) are assembled in different configurations to represent the electrolytes and electrolyte/membrane interfaces (bottom two rows of the panel) (3). (C) Equivalent circuit representation of the dynamic EP model, distinguishing the asymptotic EP model (pore formation and destruction; left gray box) (2) and its extension to the full SE (pore expansion and contraction; right gray box). The current source I_{N} in the left gray box is the pore formation and destruction term in Eq. 1. The effective voltage on each capacitor C_{N} is a representation for the pore distribution $n(r_{\mathrm{p}}, t)$ at different pore radii (not a physical voltage in the TL system model (2, 3)). Pore drift and diffusion are related to the current source I_{d} and the resistor R_{N}, respectively, as further explained in the Methods section. The local pore distribution in the EP subcircuit (C) determines the local membrane conductance G_{m} and hence the membrane current $I_{\mathrm{m}}(t)$ as input to various membrane modules M_{m} (B).

EP-subcircuit (Fig. 1 C) described below, which interacts locally at all respective membrane sites (2). The specific properties of each membrane can be dynamically adapted in this way (3).

Further, micrometer-scale electrolyte models (M_{el}) are constructed from modules for displacement (C_{el}) and conduction (R_{el}) currents (4), specifically for the extracellular (e), intracellular (i), and the space between (b) two organelle membranes. The membrane modules (M_{m}) are assigned to the specific local membrane, i.e. PM and organelle membrane, and in combination with their nearest micrometer-scale electrolyte neighbors by M_{el} models (Fig. 1 B) form a Cartesian TL. These and other basic features of the TL method are described elsewhere (2–4, 6); and all model parameters used here are given in (7). Voltages applied at the top and bottom of the system boundary provide the magnitude and direction of the uniform applied field (2). The TL used here has $\sim 2 \times 10^4$ interconnected local models with a lattice spacing of $l = 0.35\,\mu$m and is solved by Kirchhoff's laws in the time domain using Berkeley SPICE version 3f5.

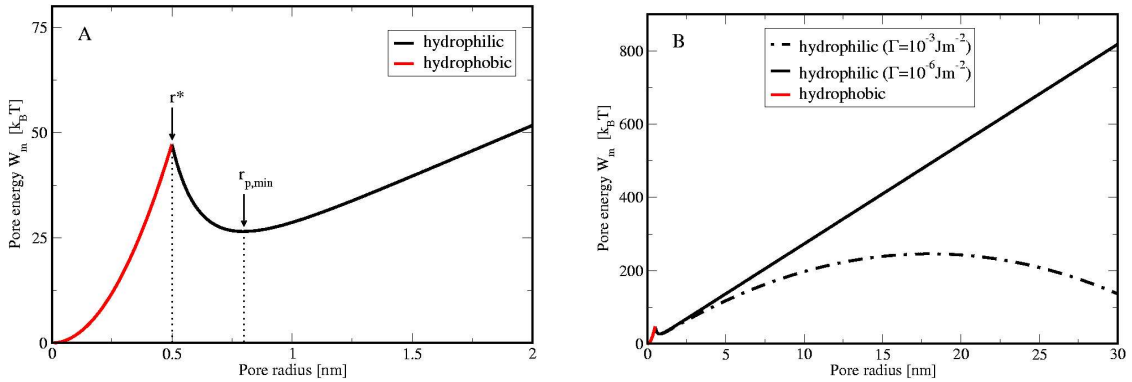

Figure 2: Mechanical pore formation energies as function of pore radius r_p (8, 9). The curve for hydrophobic pores is steeply ascending and rising to about 100 $\mathrm{k_BT}$. The curves for hydrophilic pores in bilayer membranes with line tension $\gamma = 2 \times 10^{-11}\,\mathrm{N}$ and surface tension $\Gamma = 10^{-3}\mathrm{Jm}^{-2}$ (A and B) and in cell membranes $\Gamma = 10^{-6}\mathrm{Jm}^{-2}$ (B) intersect with the hydrophobic energy at the critical radius $r^* = 0.5\,\mathrm{nm}$ and have a local minimum at the minimum pore radius of $r_\mathrm{p,min} = 0.8\,\mathrm{nm}$. While the surface tension in artificial planar bilayer membranes leads to unlimited pore growth of pores larger than $r_\mathrm{p} = 2\gamma/\Gamma$ and thus rupture, the smaller surface tension in cell membranes prompts shrinkage of pores to the minumum size.

Dynamic EP model. Cell membranes change their electrical resistance and their ionic and molecular permeabilities dramatically at elevated transmembrane potentials due to EP (10). This biophysical mechanism is hypothesized to involve transient aqueous pores. The dynamic EP model used here takes into account acquired knowledge of EP in pure lipid bilayer and cell systems, and also theoretical results obtained in previous model systems.

Specifically, it is hypothesized that the membrane poration process starts with hydrophobic pores, which due to energetic considerations should transform into hydrophilic (inverted) pores at a critical radius r^* (8). The interplay of hydrophobic and hydrophilic pore energies (Fig. 2 A) gives rise to a stabilizing, local energy minimum at a minimal hydrophilic pore radius $r_\mathrm{p,min}$ of 0.8 nm (8, 9). The hydrophobic pores are considered to be too small to significantly contribute to electrical current and as usual only the hydrophilic pores are considered.
The formation of hydrophilic conducting pores is a kinetic process over the energetic barrier at the critical radius r^* in Fig. 2 A and can plausibly be described by a rate equation, where the number of minimum–size pores $N_\mathrm{p,min} = n(r_\mathrm{p,min})\,dr_\mathrm{p}$ with $r_\mathrm{p,min} = 0.8\,\mathrm{nm}$ that is obtained from

$$\frac{\partial N_\mathrm{p,min}(r_\mathrm{p,min},t)}{\partial t} = \underbrace{A e^{B\Delta\psi^2/k_\mathrm{B}T}}_{\text{formation}} - \underbrace{\frac{N_\mathrm{p,min}(r_\mathrm{p,min},t)}{\tau_\mathrm{p}}}_{\text{destruction}} . \tag{1}$$

Eq. 1 includes the spontaneous pore formation rate per unit membrane area A, the capacitance B in units of thermal energy, and the mean pore lifetime τ_p. In particular, $A = A_0 \exp(-W(r_\mathrm{p}^*)/k_\mathrm{B}T) = 10^9\,\mathrm{s}^{-1}\mathrm{m}^{-2}$ (7) describes lipid fluctuations and an attempt rate density within a local membrane volume, which give rise to a spontaneous crossing of the energy barrier at critical radius r^* (8), and thus formation of hydrophilic pores out of hydrophobic pores. This transition is facilitated by elevated transmembrane voltages $\Delta\psi$ as the capacitance B of the local membrane volume is decreased by the entry of water into pores of critical radius, therefore the dependence $B\Delta\psi^2$ as given in (8) with $B = 20\,\mathrm{k_B T\,V^{-2}}$ (7).

While the parameters of Eq. (1), in theory, depend on specific geometrical pore models and parameters partially known only as order of magnitude estimates, all parameters of Eq. 1 can alternatively be determined from experimental data (7, 8). In Glaser *et al.* (8), for example, a quantitative analysis of the membrane current–voltage characteristics was used, whereas in Vasilkoski *et al.* (7), data from Melikov *et al.* (11) for the creation time of a single pore were used to determine A, B, and τ_p. Therefore Eq. 1 does not have free parameters. It follows from Eq. 1 that the time scale of pore formation depends on the applied field strength, the pulse duration, and the specific pulse waveform. Hence there is no absolute transmembrane voltage threshold for EP as often erroneously suggested in the literature.

Reported pore lifetimes τ_p for the destruction of conducting pores vary from milliseconds in lipid bilayers (11) to minutes in cells in suspension (10). Pore lifetime control the post–pulse electrical behavior and, together with the ion channels, the molecular transport across the membrane. At present, there is no satisfactory understanding of the basic mechanisms that give rise to this wide range of pore lifetimes. Large pores need to relax to minimum-sized pores before resealing of the membrane takes place, but this process occurs on a time scale of microseconds according to the present value of D_p. The resealing problem is difficult because of the dominance of molecular interactions between the lipids and the cell interior over externally imposed electrical interactions, viz. the small values of $\Delta\psi(t)$ after a pulse. Given the diversity of biological membrane compositions it is therefore not surprising that post-pulse recovery can vary greatly between cell (and presumably also organelle) types.

Especially long pore lifetimes appear plausible only if pore expansion, due to longer pulses, leads to pore trapping (for example by interaction with membrane proteins) or by the insertion of linear macromolecules into pores ("foot-in-the-door hypothesis", see Fig. 1 in Ref. (12)). We use here an illustrative value of $\tau_\mathrm{p} = 3$ ms for the mean lifetime, observed experimentally in lipid bilayers (11).

The evolution of the conducting, hydrophilic pores, which are formed as determined by Eq. 1, in terms of their expansion and contraction may be understood from the Smoluchowski equation (SE). The SE for the time-dependent pore distribution $n(r_\mathrm{p}, t)$ was first used for

EP theory in 1979 (13) and is

$$\frac{\partial n}{\partial t} = \underbrace{D_\mathrm{p}\frac{\partial^2 n}{\partial r_\mathrm{p}^2}}_{\text{diffusion}} + \underbrace{\frac{D_\mathrm{p}}{k_\mathrm{B}T}\left[\frac{\partial n}{\partial r_\mathrm{p}}\frac{\partial W}{\partial r_\mathrm{p}} + n\frac{\partial^2 W}{\partial r_\mathrm{p}^2}\right]}_{\text{drift}} . \tag{2}$$

From $n(r_\mathrm{p}, t)\, dr_\mathrm{p}$, the number of pores between pore radius r_p and $r_\mathrm{p} + dr_\mathrm{p}$ at any point in time t may be found. By integration over the pore radius space, an interval from the minimum pore size $r_\mathrm{p,min}$ to a maximum pore size $r_\mathrm{p,max}$, the total number of pores in any local membrane area can be found. Further, the dynamic changes of pore sizes at thermal energy $k_\mathrm{B}T$ depends on both diffusion in this pore radius space, as determined by the diffusion constant D_p, and on the drift of pores toward larger or smaller radii, depending on the time–dependent values of the pore energy $W(r_\mathrm{p}, \Delta\psi(t)) = W_\mathrm{m} + W_\mathrm{el}$. Initial conditions for Eqs. (2) and (1) are based on the equilibrium pore number $N_\mathrm{p,min}^\mathrm{eq}$ per local membrane area A_m, that is $N_\mathrm{p,min}^\mathrm{eq} = A\tau_\mathrm{p}$ (7).

For the hydrophilic pores with $r_\mathrm{p} \leq r_\mathrm{p,min}$ we use the standard expression for the mechanical pore energy W_m, that is $W_\mathrm{m} = 2\pi\gamma r_\mathrm{p} - \pi\Gamma r_\mathrm{p}^2$ (7, 8) with the edge energy γ and the surface tension Γ. The mechanical pore energy for $r_\mathrm{p} \leq r_\mathrm{p,min}$ is dominated by steric repulsion (8, 9). Any pore of such smaller size will therefore rapidly expand towards the minimum pore size (Fig. 2 B) motivating our approach to neglect pore sizes below $r_\mathrm{p,min}$ in Eq. 2.

While Γ in artificial planar bilayer membranes is typically large ($10^{-3}\,\mathrm{Jm}^{-2}$ (14)), which may lead to irreversible pore growth for pores with radius larger than $r_\mathrm{p} = 2\gamma/\Gamma$ and hence destruction of the bilayer, the surface tension Γ for cells, as discussed here, is typically small, 10^{-6} to $10^{-5}\,\mathrm{Jm}^{-2}$ (15, 16). This case leads to $\Gamma \ll \gamma/d_\mathrm{m}$, already discussed in Ref. (8) in relation to reversible electrical breakdown (REB). In other words, infinite pore growth for cell membranes is practically not possible based on the SE model, all pores eventually return to the minimum radius $r_\mathrm{p,min}$ and decay. Therefore, the breakdown is called reversible electrical breakdown associated with a transient high-conductance state of the membrane.

Further, W_el is the electrical pore energy contribution, which depends on the transmembrane potential $\Delta\psi(t)$ and thus changes with time. Early expressions for W_el recognize the capacitive energy concept (17) and the actual electric current through a cylindrical pore which is altered by Born energies (18) and the spreading resistance (14). As those expressions may actually be applied only to small pores with a radius $r_\mathrm{p} \leq d_\mathrm{m}$ (8), we use

$$W_\mathrm{el} = -\int_0^{r_\mathrm{p}} \frac{F_\mathrm{max}}{1 + r_\mathrm{h}/(r + r_\mathrm{t})}\Delta\psi^2 dr \tag{3}$$

with $F_\mathrm{max} = 6.9\times10^{-10}\,\mathrm{N/V^2}$, $r_\mathrm{h} = 0.95\,\mathrm{nm}$, and $r_\mathrm{t} = 0.23\,\mathrm{nm}$. This interpolating expression is given in Ref. (19) and results from Maxwell stress tensor based numerical simulations and allows for the simultaneous treatment of small and large pores.

Asymptotic EP models (9) neglect pore expansion and shrinkage equivalent to $D_\mathrm{p} = 0$ in

Eq. 2. This is sufficient for nanosecond electric field pulses but not for longer conventional EP pulses (7, 20). The asymptotic EP model, as given by Eq. 1, has been previously represented by an equivalent electric circuit (2), and is shown in Fig. 1 C in the left gray box (compare with Fig. 5 in (2)). As previously explained, the unit capacitor at the pore node is $C_{\mathrm{N}} = 1$, and the current source I_{N} represents the rate of change of $N_{\mathrm{p,min}}$ as given by the right hand side of Eq. 1 (2).

In Fig. 1 C (right gray box) we introduce a generalized equivalent circuit that is used to solve the full SE in Eq. 2 and takes into account pore size dynamics in terms of electrical circuits. For this purpose we discretize the pore radius space, which ranges from the minimum pore size $r_{\mathrm{p,min}}$ to the maximum pore size $r_{\mathrm{p,max}}$, into bins of size $dr_{\mathrm{p}} = 0.05\,\mathrm{nm}$ ($[r_{\mathrm{p,min}}, r_{\mathrm{p,min}} + dr_{\mathrm{p}}, ..., r_{\mathrm{p,max}}]$) and consider the pore distribution $n(r)$ in each discretized bin.

The equivalence of the electric circuit in Fig. 1 C and the SE of Eq. 1 is as follows: The first term of Eq. 2 describing diffusion in pore radius space is represented by a resistor $R_{\mathrm{N}} = (dr_{\mathrm{p}})^2/D_{\mathrm{p}}$ between neighboring nodes of pore radius r_{p} and $r_{\mathrm{p}} + dr_{\mathrm{p}}$. The drift term in Eq. 2 is taken into account by an active current element I_{d} (Fig. 1 C), which is given between succeeding pore radii r_{p} and $r_{\mathrm{p}} + dr_{\mathrm{p}}$ by

$$I_{\mathrm{r_p,r_p+dr_p}} = \frac{D_{\mathrm{p}}}{2k_{\mathrm{B}}T(dr_{\mathrm{p}})^2}\left[n(r_{\mathrm{p}} + dr_{\mathrm{p}}) + n(r_{\mathrm{p}})\right]\left[W(r_{\mathrm{p}} + dr_{\mathrm{p}}) - W(r_{\mathrm{p}})\right]\,. \tag{4}$$

Eq. 4 accounts for the net rate of pores appearing and disappearing in each bin, as pores expand or contract within a local membrane area in response to the pore energies, $W(r_{\mathrm{p}})$. These depend on the instantaneous values of the local transmembrane voltage $\Delta\psi$. Eq. 4 is a standard mathematical expression for the discretization of the drift term of Eq. 2 (see, for example, Appendix 2 of Ref (21)). At each node r_{p} in pore radius space there is an I_{d}–influx (from bin $r_{\mathrm{p}} - dr_{\mathrm{p}}$) and an I_{d}–efflux (to bin $r_{\mathrm{p}} + dr_{\mathrm{p}}$), such that the expression $\partial n(r_{\mathrm{p}}, t)/\partial t|_{\mathrm{drift}}$ of Eq. 2 with both the linear and the quadratic derivatives of the pore energy W is equivalent (in the limit $dr_{\mathrm{p}} \to 0$) to $I_{\mathrm{r_p-dr_p,r_p}} - I_{\mathrm{r_p,r_p+dr_p}}$ at each pore radius bin r_p. A mathematical proof of this equivalence is provided in Ref. (22).

The maximum pore size r_{max} used in the present paper is 5 nm. The dynamic EP circuit is solved for every local membrane module (M_{m}), from which we obtain the time-dependent membrane pore conductance G_{m} (Eq. 6 in (7)) and hence the local pore current $I_{\mathrm{m}} = G_{\mathrm{m}}\,\Delta\psi(t)$ at the PM and all organelle membranes (3, 7), respectively, as input into the membrane modules M_{m}, see Fig. 1 B. The EP subcircuits in Fig. 1 C thus interact locally with the distributed TL of the cell system.

Appendix A

Dynamic EP in a planar membrane patch. Here we describe the EP behavior for a small, planar membrane patch of area $A_{\mathrm{m}} = 3\,\mu\mathrm{m}\times 3\,\mu\mathrm{m}$. The results serve as a validation of

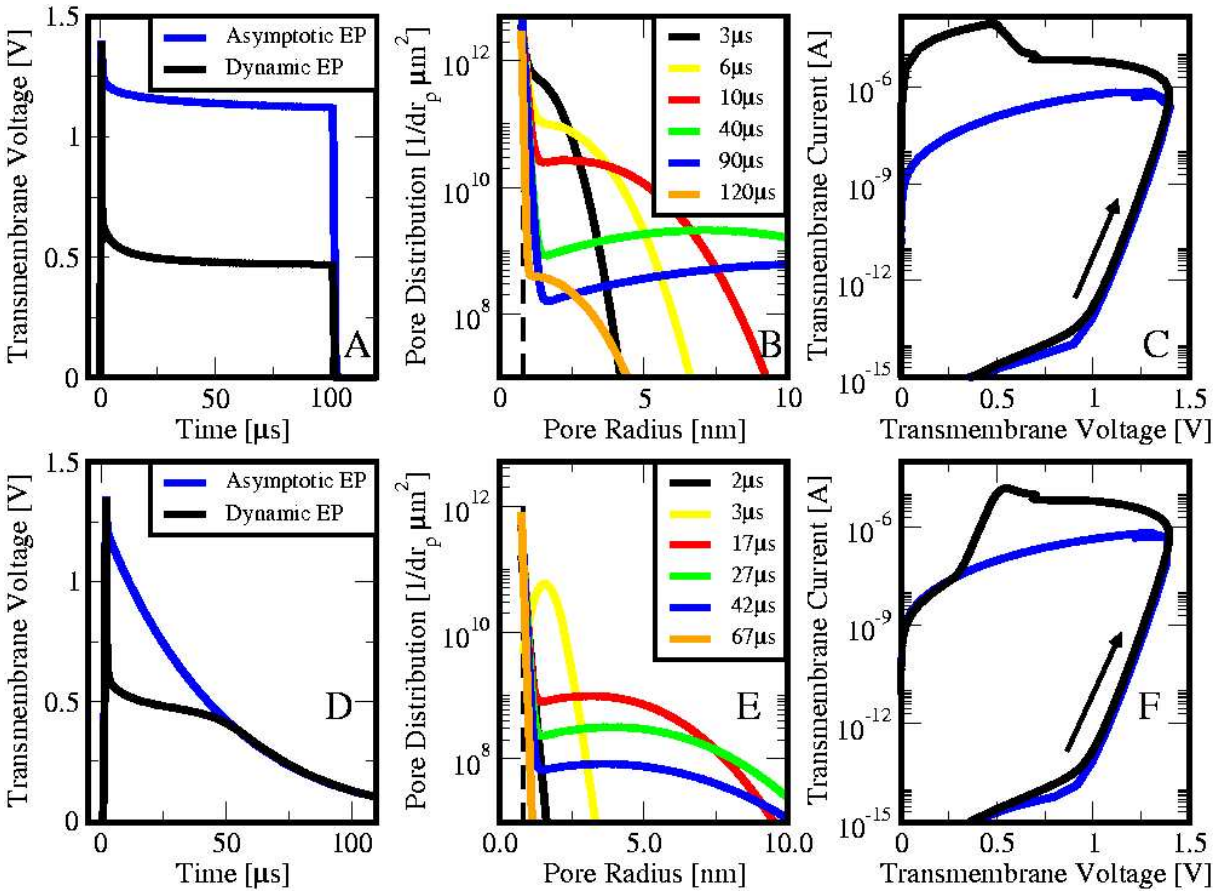

Figure 3: 1D membrane patch (area A_{m} =3 μm × 3 μm) response to (A–C) trapezoidal pulse (E^0_{app} =1 kV/cm, 100 μs duration, 1 μs rise and fall times and (D–F) exponential pulse (E^0_{app} =1 kV/cm, τ_{pulse} = 40 μs, 1 μs rise time): (A, D) $\Delta\psi_{\mathrm{PM}}$ initially charges with time constant $\tau = 0.1\,\mu$s and reaches the peak at $\Delta\psi \approx 1.4\,V$. The membrane conductance increases due to pore formation, and pore expansion then causes a rapid decay to $\Delta\psi \approx 0.5$ V. Then, $\Delta\psi$ exhibits a voltage-regulating effect with a plateau-like behavior, notably in (D), due to dynamic pore-size changes (23). The asymptotic EP model (blue) with no pore expansion has distinct different behavior, with a much higher value of $\Delta\psi_{\mathrm{PM}}$ during the pulse since pores do not expand and the additional creation of pores is strongly suppressed. (B, E) Time-dependent pore distributions: pores created at minimum size ($r_{\mathrm{p,min}} = 0.8$ nm, dashed line) expand to larger radii and subsequently return to $r_{\mathrm{p,min}}$. The pore distribution evolves during the entire pulse, and larger pores appear for the trapezoidal pulse (B). (C, E) The membrane current - voltage ($I_{\mathrm{PM}} - \Delta\psi_{\mathrm{PM}}$) characteristics shows conductance hysteresis (arrow indicates time direction of the pulse). The strong increase in I_{PM} above 0.8 – 1 V marks the EP onset. After the peak, I_{PM} continues to increase despite a drop in $\Delta\psi_{\mathrm{PM}}$ due to pore expansion. In contrast, the lack of pore expansion in the asymptotic model limits I_{PM}, hence the SE model of EP (black) has a larger membrane conductance after the peak during voltage regulation of $\Delta\psi_{\mathrm{PM}}$. For later times, I_{PM} decreases as pores shrink and subsequently decay.

solving EP models (7, 23) by TLs and both confirm and extend our previous understanding of the EP features. In particular, Fig. 3 shows the salient features of EP due to an exponential 1 kV/cm, $\tau_{\text{pulse}} = 40\,\mu$s pulse with a 1 μs rise time based on the planar membrane patch model described in Ref. (7), but solved here by the TL method.

Fig. 3 A shows that with the onset of the pulse, $\Delta\psi_{\text{PM}}$ increases with time constant $\tau_{\text{PM}} = 0.1\,\mu$s. Even though EP sets in at $\Delta\psi_{\text{PM}} \approx 0.8 - 1$ V for this particular pulse, as indicated by a strong increase in membrane current (Fig. 3 C), the transmembrane potential continues to rise and a burst of pore creation continues until a peak at $\Delta\psi_{\text{PM}} \approx 1.4$ V. The membrane does not maintain this value for long, as it is well above normal physiological magnitudes. Instead, a sudden drop in $\Delta\psi_{\text{PM}}$ that is associated with a reversible high conductance state of the membrane (REB)) occurs (7, 23). Expansion of pores subsequently causes a further increase in membrane conductivity.

Remarkably, $\Delta\psi_{\text{PM}}$ does not track the time–dependence of the external exponential pulse (Fig. 3 A) after the peak. Instead $\Delta\psi_{\text{PM}}$ reaches a plateau-like state around $\Delta\psi_{\text{PM}} \approx 0.5$ V. What happens at this particular transmembrane voltage? As demonstrated in Fig. 2B of our paper, the pore energy W has a maximum at a pore radius of about 2 nm such that dynamic changes in the pore distribution results simultaneously in both pore shrinkage for pores which have a radius below 2 nm and pore expansion for pores which have a radius above 2 nm. This quasi-plateau therefore reflects a voltage regulating effect due to an agile response of dynamic pores (23).

But then why does the plateau-like state occur? The applied field decreases during the exponential pulse, which tends to decrease $\Delta\psi_{\text{PM}}$ as well. However, most previously expanded pores respond by shrinking, which increases the membrane resistance such that voltage division with the electrolyte resistance inhibits a decrease of $\Delta\psi_{\text{PM}}$. By the end of the plateau, the formerly large pores have shrunk to near minimum size (0.8 nm) and further shrinkage in response to a decreasing electric field is not possible. Consequently, $\Delta\psi_{\text{PM}}(t)$ then follows $E_{\text{app}}(t)$ and exhibits the exponential time-dependence of the external pulse.

This voltage regulation effect fundamentally depends on a $\Delta\psi_{\text{PM}}(t)$ –sensitive pore distribution (7, 23). Consequently, the voltage regulation effect would be absent if pore size change was suppressed (D_{p}=0) such as in the asymptotic EP model. The above shape of the time–dependent transmembrane voltage: rise, peak, sudden drop, plateau, decay, has been observed in different systems. For example, a comprehensive experiment in BLM showed that both REB and rupture (mechanical breakdown) can be caused in the same membrane preparation by varying only the magnitude of a 400 ns pulse (24). The main features of these experiments are consistent with an EP theory based on stochastic pore creation followed by pore expansion and contraction described by the SE (25). Other studies with BLM systems also demonstrate REB (26). REB was also demonstrated in the double membrane of a giant algal cell (27). Finally, REB was demonstrated in a widely used epithelial tissue (viable frog skin) and found to cause no measurable damage (28). Thus, although not presently a focus of EP research, REB has been established as a feature of reversible EP in artificial planar bilayers, membranes, cell membranes and tissue.

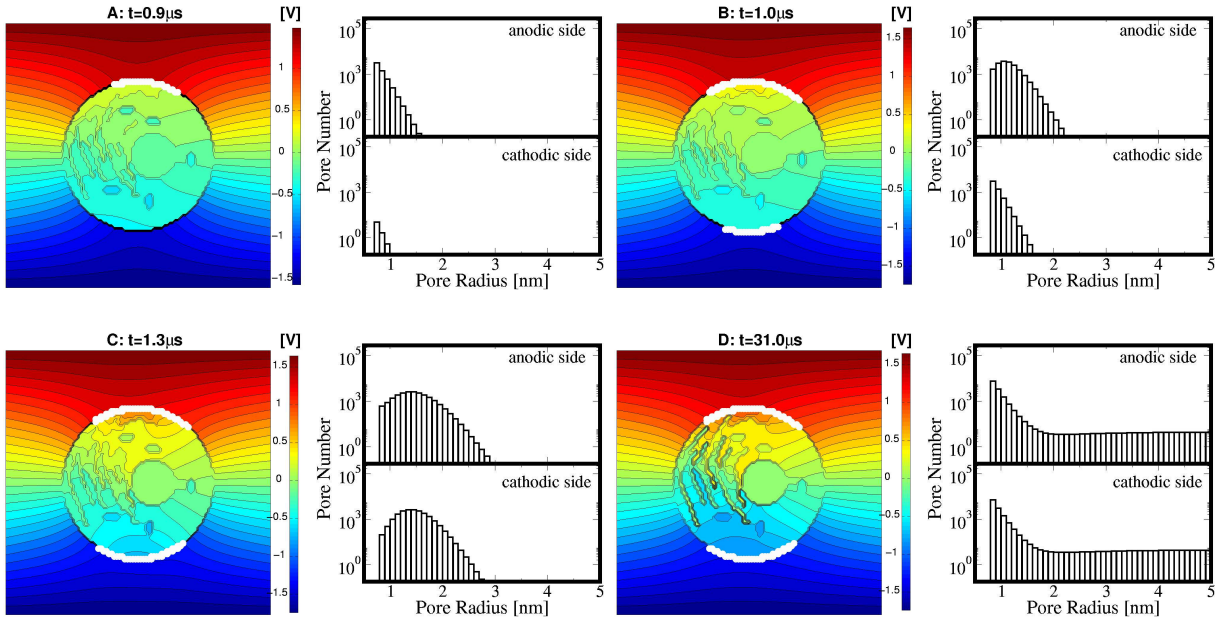

Figure 4: (Left panel) Distributed electrical response of the cell model to a trapezoidal pulse ($E^0_{\mathrm{app}} = 1\,\mathrm{kV/cm}$, $100\,\mu\mathrm{s}$ duration, $1\,\mu\mathrm{s}$ rise and fall times); colorbar shows the potential scale. White dots are local membrane sites with ≥ 50 pore (corresponding to a pore density of $N_{\mathrm{p}} = 10^{13}\mathrm{m}^{-2}$). (Right panel) Pore histograms for the anodic and cathodic membrane side give the total number of pores and their size within intervals of 0.1 nm. (A) EP starts at $t = 0.9\,\mu\mathrm{s}$ on the anodic side, followed at $t = 1.0\,\mu\mathrm{s}$ on the cathodic side in (B). Pore expansion also starts initially at the anodic side. (C) Significant pore expansion at $t = 1.3\,\mu\mathrm{s}$ at both the anodic and cathodic side; intracellular equipotential lines reveal the emergence of electric fields in the cell interior. (D) At $t = 31\,\mu\mathrm{s}$, the pore histograms regain a maximum at $r_{\mathrm{p,min}}$, but simultaneously show non-equilibrium tails toward larger pores. See FIG. 2 and related text in the paper for comparison.

Dynamic changes in the $\Delta\psi_{\mathrm{PM}}$–dependent pore distribution $n(r_{\mathrm{p}}, t)$ are shown in Fig. 3 B. Pore creation occurs at the minimum pore size $r_{\mathrm{p,min}} = 0.8\,\mathrm{nm}$ that allows for electrical conduction. Subsequent expansion and shrinkage of pores is evident as the pulse progresses. The importance of creating larger pores has long been recognized, e.g., pores larger than 5 nm are required for DNA to enter a cell (19). However, DNA electrophoresis and partial occlusion of pores may impose additional forces, and thus augment pore expansion (29) not reflected in our model. After the end of the plateau and during the exponential decay of $\Delta\psi_{\mathrm{PM}}(t)$, the pore distribution shrinks on a microsecond time scale and becomes dominated by minimum–size pores. Hence long–lived pores are not expected to be larger than 1 nm, underlying the observed behavior that larger molecules can only be forced into cells during the EP pulse, not after (30, 31) for reversible EP conditions.

Fig. 3 C illustrates the non-linear current-voltage (I_{PM}–$\Delta\psi_{\mathrm{PM}}$) characteristics of the mem-

brane, demonstrating hysteretic electric behavior, viz. the possibility of having two different I_{PM} values at the same $\Delta\psi_{\mathrm{PM}}$. EP thus introduces a memory effect, and significant membrane conductance increases occur at both (i) the onset of EP at $\Delta\psi_{\mathrm{PM}} \approx 0.8 - 1\,\mathrm{V}$ and (ii) pore expansion after the peak at $\Delta\psi_{\mathrm{PM}} \approx 1.4\,\mathrm{V}$. Remarkably, the membrane current I_{PM} continues to grow after the peak despite a drop in $\Delta\psi_{\mathrm{PM}}$, which is only possible if pores expand and thus cause an increase in membrane conductance. An important interpretation of the model's behavior is thus that the membrane conductance changes during the entire pulse as pores dynamically change their size.

Appendix B

Trapezoidal Pulses. The comparison with the trapezoidal 1 kV/cm pulse with a 100 μs duration and 1 μs rise and fall times (Fig. 3 D–F) shows similar behavior for the $\Delta\psi_{\mathrm{PM}}$-transients: $\Delta\psi_{\mathrm{PM}}$ drops to a plateau after its peak that persists for the entire pulse, despite dynamic changes in the pore distribution that continue during the duration of the pulse. Thus, even if $\Delta\psi_{\mathrm{PM}}$ does not change significantly, there is a continual force in pore radius space to change pore radii. Elevated values of $\Delta\psi_{\mathrm{PM}}$ persist for longer for the trapezoidal pulse than for the exponential pulse. This allows for the creation of larger pores as can be seen in the pore distribution (Fig. 3 B). After the pulse, the pore distribution rapidly ($\sim \mu$s) shrinks to a distribution of minimum–size pores; hence long–lived pores are not expected to be larger than 1 nm (30). The hysteretic current-voltage (I_{PM}-$\Delta\psi_{\mathrm{PM}}$) characteristics in (Fig. 3 C) consistently shows higher membrane currents due to creation of larger pores.

Fig. 4 shows the distributed electric response to the trapezoidal 1 kV/cm with a 100 μs pulse duration. The results compare well with those obtained for the exponential pulse in Fig. 3 of our paper, demonstrating the robustness of the EP mechanism and suggesting that our conclusions, with respect to emergence of intracellular electric fields, its strength, and its influence on organelles as well as for the EP asymmetry, are also valid for other waveforms.

Acknowledgments

This work was supported by National Institutes of Health (R01-GM63857), Aegis Industries, and a Graduate Research Fellowship to K.C.S. from the National Science Foundation. We thank A. G. Pakhomov for helpful insights, K. G. Weaver for computer support and R. S. Son for technical support.

References

1. Rizzuto, R., P. Pinton, W. Carrington, F. S. Fay, K. E. Fogarty, L. M. Lifshitz, R. A. Tuft, and T. Pozzan, 1998. Close contacts with the Endoplasmic Reticulum as Determinants of Mitochondrial Ca^{2+} Responses. *Science* 280:1763–1766.

2. Stewart, D. A., T. R. Gowrishankar, and J. C. Weaver, 2004. Transport lattice approach to describing cell electroporation: use of a local asymptotic model. *IEEE Transactions on Plasma Science* 32:1696–1708.

3. Gowrishankar, T. R., A. T. Esser, Z. Vasilkoski, K. C. Smith, and J. C. Weaver, 2006. Microdosimetry for conventional and supra-electroporation in cells with organelles. *Biochem. Biophys. Res. Commun.* 341:1266–1276.

4. Gowrishankar, T. R., and J. C. Weaver, 2003. An approach to electrical modeling of single and multiple cells. *Proc. Nat. Acad. Sci.* 100:3203–3208.

5. Esser, A. T., T. R. Gowrishankar, K. C. Smith, and J. C. Weaver, 2007. Towards solid tumor treatment by irreversible electroporation: Intrinsic redistribution of fields and currents in tissue. *Tech. Cancer Res. Treat.* 6:261–273.

6. Smith, K. C., T. R. Gowrishankar, A. T. Esser, D. A. Stewart, and J. C. Weaver, 2006. The spatially distributed, dynamic transmembrane voltage of cells and organelles due to 10 ns pulses: meshed transport networks. *IEEE Trans Plasma Sci* 34 (4):1480–1493.

7. Vasilkoski, Z., A. T. Esser, T. R. Gowrishankar, and J. C. Weaver, 2006. Membrane electroporation: The absolute rate equation and nanosecond time scale pore creation. *Phys. Rev. E* 74:021904–1–021904–12.

8. Glaser, R. W., S. L. Leikin, L. V. Chernomordik, V. F. Pastushenko, and A. I. Sokirko, 1988. Reversible electrical breakdown of lipid bilayers: formation and evolution of pores. *Biochim. Biophys. Acta* 940:275–287.

9. Neu, J. C., and W. Krassowska, 1999. Asymptotic Model of Electroporation. *Phys. Rev. E* 59:3471–3482.

10. Weaver, J. C., 2003. Electroporation of biological membranes from multicellular to nano scales. *IEEE Trans. Dielect. Elect. Ins.* 10:754–768.

11. Melikov, K. C., V. A. Frolov, A. Shcherbakov, A. V. Samsonov, Y. A. Chizmadzhev, and L. V. Chernomordik, 2001. Voltage–induced nonconductive pre–pores and metastable pores in unmodified planar bilayer. *Biophys. J.* 80:1829–1836.

12. Weaver, J. C., 1993. Electroporation: A General Phenomenon for Manipulating Cells and Tissue. *J. Cellular Biochem.* 51:426–435.

13. Pastushenko, V. F., Y. A. Chizmadzhev, and V. B. Arakelyan, 1979. Electric Breakdown of Bilayer Membranes: II. Calculation of the Membrane Lifetime in the Steady-State Diffusion Approximation. *Bioelectrochem. Bioenerget.* 6:53–62.

14. Weaver, J. C., and Y. A. Chizmadzhev, 1996. Electroporation. *In* C. Polk, and E. Postow, editors, Handbook of Biological Effects of Electromagnetic Fields, CRC Press, Boca Raton, 247–274. 2nd edition.

15. Dai, J., and M. P. Sheetz, 1995. Regulation of endocytosis, exocytosis, and shape by membrane tension. *Cold Spring Harb. Symp. Quant. Biol.* 60:567–571.

16. Henon, S., G. Lenormand, A. Richert, and F. Gallet, 1998. A new determination of the shear modulus of the human erytrocyte membrane using optical tweezers. *Biophys. J.* 76:1145–1151.

17. Abidor, I. G., V. B. Arakelyan, L. V. Chernomordik, Y. A. Chizmadzhev, V. F. Pastushenko, and M. R. Tarasevich, 1979. Electric Breakdown of Bilayer Membranes: I. The Main Experimental Facts and Their Qualitative Discussion. *Bioelectrochem. Bioenerget.* 6:37–52.

18. Pastushenko, V. F., and Y. A. Chizmadzhev, 1982. Stabilization of Conducting Pores in BLM by Electric Current. *Gen. Physiol. Biophys.* 1:43–52.

19. Smith, K. C., J. C. Neu, and W. Krassowska, 2004. Model of creation and evolution of stable electropores for DNA delivery. *Biophys. J.* 86:2813–2826.

20. Esser, A. T., T. R. Gowrishankar, K. C. Smith, and J. C. Weaver, 2009. Towards solid tumor treatment by nanosecond pulsed electric fields. *Tech. Cancer Res. Treat.* 8(4):289–306.

21. Kurnikova, M. G., R. D. Coalson, P. Graf, and A. Nitzan, 1999. A lattice relaxation algorithm for three-dimensional Poisson-Nernst-Planck theory with application to ion transport through the Grmaicidin A channel. *Biophys. J.* 76:642–656.

22. Smith, K. C., 2006. Modeling cell and tissue electroporation. Massachusetts Institute of Technology. SM Thesis (Online: http://hdl.handle.net/1721.1/35301).

23. Freeman, S. A., M. A. Wang, and J. C. Weaver, 1994. Theory of Electroporation for a Planar Bilayer Membrane: Predictions of the Fractional Aqueous Area, Change in Capacitance and Pore-Pore Separation. *Biophys. J.* 67:42–56.

24. Benz, R., F. Beckers, and U. Zimmermann, 1979. Reversible Electrical Breakdown of Lipid Bilayer Membranes: A Charge-Pulse Relaxation Study. *J. Membrane Bio.* 48:181–204.

25. Barnett, A., and J. C. Weaver, 1991. Electroporation: A Unified, Quantitative Theory of Reversible Electrical Breakdown and Rupture. *Bioelectrochem. and Bioenerg.* 25:163–182.

26. Wilhelm, C., W. M, U. Zimmermann, and R. Benz, 1993. Kinetics of pore size during irreversible electrical breakdown of lipid bilayer membranes. *Biophys. J.* 64:121–128.

27. Benz, R., and U. Zimmermann, 1980. Relaxation Studies on Cell Membranes and Lipid Bilayers in the High Electric Field Range. *Bioelectrochem. and Bioenerg.* 7:723–739.

28. Powell, K. T., A. W. Morgenthaler, and J. C. Weaver, 1989. Tissue Electroporation: Observation of Reversible Electrical Breakdown in Viable Frog Skin. *Biophys. J.* 56:1163–1171.

29. Pastushenko, V. P., and Y. A. Chizmadzhev, 1992. Energetic Estimations of the Deformation of Translocated DNA and Cell Membrane in the Course of Electrotransformation. *Biol. Mem.* 6:287–300.

30. Kinosita, Jr., K., and T. Y. Tsong, 1977. Formation and Resealing of Pores of Controlled Sizes in Human Erythrocyte Membrane. *Nature* 268:438–441.

31. Sukharev, S. I., V. A. Klenchin, S. M. Serov, L. V. Chernomordik, and Y. A. Chizmadzhev, 1992. Electroporation and electrophoretic DNA transfer into cells. The effect of DNA interaction with electropores. *Biophys. J.* 63:1320–1327.